ORIGINAL RESEARCH

Active Hydrophilic Graphene Oxide Nanocomposites Delivery Mediated by Adipose-Derived Stem Cell for Elevated Photothermal Therapy of Breast Cancer

Zhangsong Peng [iD][1],*, Qiang Chang[1,2],*, Malcolm Xing[2], Feng Lu[1]

[1]Department of Plastic and Reconstruction Surgery, Nanfang Hospital, Southern Medical University, Guangzhou, 510515, People's Republic of China; [2]Department of Mechanical Engineering, University of Manitoba, Children's Hospital Research Institute of Manitoba, Winnipeg, Manitoba, R3T 2N2, Canada

*These authors contributed equally to this work

Correspondence: Malcolm Xing, Department of Mechanical Engineering, University of Manitoba, Children's Hospital Research Institute of Manitoba, Winnipeg, Manitoba, R3T 2N2, Canada, Email malcolm.xing@umanitoba.ca; Feng Lu, Department of Plastic and Reconstruction Surgery, Nanfang Hospital, Southern Medical University, Guangzhou, 510515, People's Republic of China, Email doctorlufeng@hotmail.com

Purpose: Graphene oxide (GO) and its derivatives have recently been identified as promising candidates for early disease diagnosis and therapy. However, the physiological stability and precise launch requirements present limitations on further clinical practices. Adipose-derived stem cells (ADSCs) were employed as an unobstructed biological vehicle to address the validate this ADSC-based tumor-targeting system for highly efficient GO delivery combined with two-stage NIR radiation for superior tumor ablation.

Methods: GO was modified with poly-ethylene glycol (PEG) and folic acid (FA). Afterward, the GO nanocomposite was internalized into ADSCs. The GO-PEG-FA-laden ADSCs were injected into the tail veins of the tumor-bearing mice. Subsequently, first-stage NIR radiation was utilized to disrupt the ADSCs for GO-PEG-FA release. After this, the heat generated by secondary-stage NIR radiation destroy the malignant cells and shrink the tumor, and the cascade process could be recycled until complete tumor ablation if necessary.

Results: The GO-PEG-FA nanocomposite exhibited negligible cytotoxicity and could be internalized into ADSCs to target specific tumor sites after 32 days of intravenous injection. The nanocomposite was released from the ADSCs and taken up into cancer cells again with the assistance of FA after the first dose of near-infrared radiation. Then, the second radiation dose could directly strike the cancer cell for cancer ablation.

Conclusion: In summary, we reported a stem cell-based anticancer system that used GO-PEG-FA-laden ADSCs for breast cancer therapy through NIR treatment in mice potentially opens a new avenue not only to address precise drug targeting in tumor therapy, but also future clinical practice in diverse areas.

Keywords: graphene oxide, adipose-derived stem cells, nanocomposite, photothermal therapy, breast cancer

Introduction

Breast cancer leads as the most frequent and lethal cancer among females in every region in the world, with nearly 12.5% of women suffering from breast cancer during their lifetime.[1] Although alternative and combined chemoradiotherapy and surgical excision have contributed to cancer clearance and survival rates, these traditional techniques still barely satisfy the financial impact, aesthetic requirements, and complications.[2] The development of nanocarriers and nanodrugs has drawn great attention because of their ability to deliver anticarcinogens based on passive targeting and enhanced permeability and retention, injectable administration, and minimal collateral damage to normal tissue[3,4].

Carbonaceous nanomaterials such as carbon nanotubes, graphene oxide (GO), and their derivatives including GO aerogels[5] have been proven to be promising cancer-selective drug carriers for anticancer drugs, such as doxorubicin,[6]

paclitaxel,[7] and oligonucleotides,[8] owing to their large surface area and π–π stacking. However, the non-specific cytotoxicity of these nanomaterials along with the resistance of the current anticarcinogens, reduces the full therapeutic achievement.[9] Recently, photothermal therapy (PTT) based on GO and near-infrared laser radiation (NIR, 650–900 nm wavelength) has been proposed as a potential and feasible strategy for cancer ablation because of its pronounced heat generation efficiency and the readily modifiable edge groups of GO as compared to its carbon nanotube counterparts.[10–14] The selective attachment of a GO nanocomposite to malignant cells ensures the elevated sensitization of the targeted cells to the NIR light, which is non-absorptive to normal cells, and the superior capability of the strong absorption of NIR and thermal energy conversion based on delocalized electron orbitals has prompted the exploration of GO in the past decade.[13] Nevertheless, the stability of GO in a physiological environment is dramatically attenuated by the electronic charge and nonspecific protein binding, which leads to GO aggregation. Several efficient yet green reductionist surface modification approaches and polymers have been utilized to improve the stability of GO in physiological solutions, such as polyethylene glycol (PEG),[15] hyaluronic acid,[3] curcumin[16] and protein,[17,18] and higher cellular uptake efficiencies have been verified with in vitro studies. Furthermore, exclusive receptors such as the folic acid receptor[19] and cluster determinant 44[20] have been overexpressed in various malignant cells, with limit the distribution in normal cells, and the specific receptor-mediated GO delivery system has seized the spotlight owing to its more efficient transfer and targeting.[10,21] However, hard nanocomposites rely on the passive transfer from circulation to target cancer tissue, and the velocity of blood flow suffers a "cliff-like drop" in a liver sinusoid (from 10–100 cm s-1 to 0.2–0.8 cm s-1), leading to the sequestration, accumulation, and clearance of most of the nanocomposite from circulation by the mononuclear phagocyte system in vivo (MPS, including Kupffer cells, B cells, and endothelial cells in the liver and spleen). Moreover, it is worth noting that a significant accumulation by the MPS still occurred regardless of surface physicochemical modification (for example, PEGylated modification).[22]

Given the complex circulating and rigorous clearance system, another method needs to be found to ensure a sufficient quantity of the nanocomposite targeting the desired cancer site. Recently, nanoparticle delivery mediated by cancer-tropic cells has received particular attention because of the minimal immunogenicity and clearance rate by the MPS, as well as the efficient targeting attributed to tumor tropism by the chemotactic gradient. The advanced delivery of paclitaxel to a malignant brain tumor was demonstrated by a neutrophil-mediated liposome nanocomposite with the ability to traverse the blood–brain barrier.[5] Enhanced tumor accession and ablation were also achieved by gold nanorod loading in macrophages for PTT.[23] Nevertheless, the proliferation capability of these vectors is strictly limited in vitro, and the short lifespan and complex purification process also detract from practical applications.[24] In addition to inflammation cells, the aborigines in circulation, another cancer-tropic cell type, mesenchymal stem cells (MSCs), are particularly appealing and have been widely investigated recently because of their equally powerful tumor tropism. In addition, their convenience and clinical potential are enhanced by their near-infinite proliferation ability.

The considerable targeting and anticancer capabilities of bone marrow-MSCs (BMMSCs) endocytosed with nano-cures have been validated in different cancer models because of their retained homing ability and low immunogenicity after loading. In addition, live cells can transverse the barely permeable barriers to designed targets, which passive nanocomposite delivery cannot normally circumvent.[25,26] However, BMMSC extraction from bone marrow requires a painful surgical process, and an ex vivo culture is indispensable for sufficient cell numbers because of the restricted volume that can be extracted from marrow each time. Moreover, a chromosomal abnormality in BMMSCs was reported during cell passaging.[27,28] Furthermore, it is worth noting that the paradoxical biosafety of BMMSCs in the tumor microenvironment is not yet conclusive. Both pro- and anti-tumorigenic functions have been raised and explored systemically.[29–31] Most reports have fully documented the prominently efficient targetability of BMMSCs loaded with nanocomposites for thermal therapy. Yet, few dug deeper into the stem cell destiny after radiation and the optimization of PTT.

The inherent concerns with BMMSCs led us to consider whether other types of MSCs are more clinically applicable for anti-tumorigenic agent delivery to the tumor site. Our group previously demonstrated another MSC type from adipose tissue, adipose-derived stem cells (ADSCs), which exhibited active migration into the wound and tumor tissue via an inflammatory gradient, with an intrinsic tumor-tropism behavior similar to that of BMMSCs.[32,33] In addition, solid evidence has revealed the differences between BMMSCs and ADSCs, with ADSCs having several advantages over
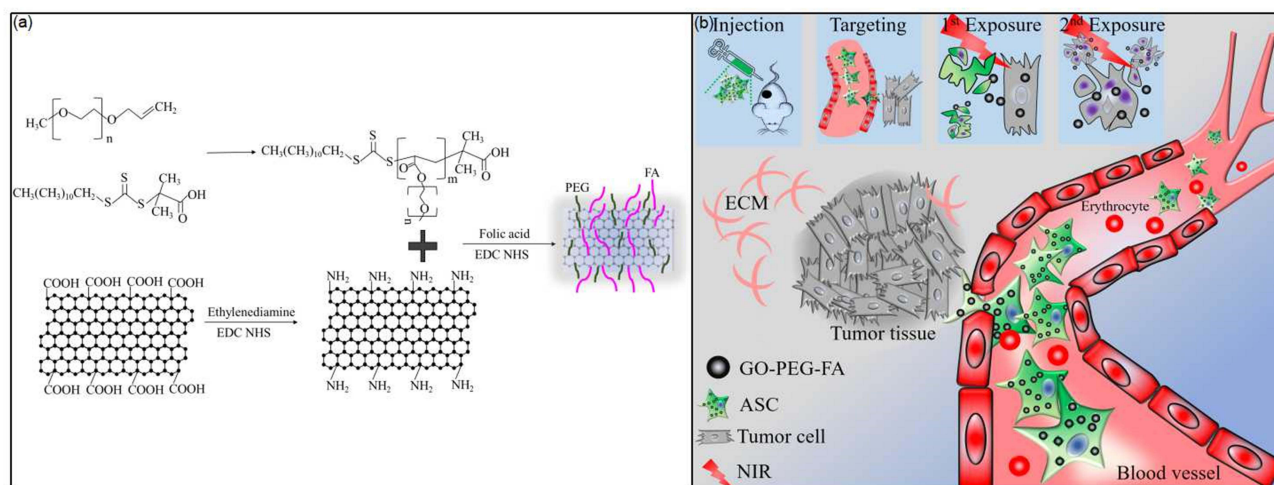
Figure 1 (**a**) Synthesis process of GO-PEG-FA nanocomposites. (**b**) Specific tumor-targeting by active ADSCs delivery and two-stage NIR radiation-controlled nanocomposite release for enhanced tumor therapy.
Abbreviations: GO, Graphene oxide; PEG, poly-ethylene glycol; FA, folic acid; ADSCs, Adipose-derived stem cells; NIR, near-infrared laser radiation.

BMMSCs. (1) ADSCs possess a high extraction potential and can be easily and repeatedly isolated from liposuction, which has been a well-established surgical procedure in plastic and aesthetic practice for decades, with "medical waste" becoming "regenerative gold". (2) Liposuction is a minimally invasive procedure that is far less painful than bone marrow aspiration, and a commercial sorter for ADSCs is currently available in the market. (3) The colony unit formation speed of ADSCs is almost 7-fold that of BMMSCs, with approximately 23.6% if BMMSCs undergoing senescence at early passaging (the ration of ADSCs is 5%), and ADSCs possess higher proliferation than BMMSCs.[34] (4) ADSCs are more effective from the perspective of immunomodulatory activity.[35] (5) Because a small piece of adipose tissue is sufficient for an abundant reservoir of stem cells, ADSCs are believed to be more favorable for elderly patients who also suffer the highest morbidity rate of cancer. However, currently, cell-mediated delivery strategies for nanocomposites based on ADSCs are still rare, and the critical malignant transformation of stem cells in the tumor microenvironment is still unclear.

Herein, we propose the vectorization of PEGylated GO with folic acid (FA) decoration by ADSC-mediated active targeting for breast cancer ablation combined with two-stage NIR radiation for PTT (Figure 1). Specifically, GO was modified with PEG and FA (GO-PEG-FA). The former polymer provided a hydrophilic shield to stabilize the GO dispersion in a physical solution, as well as in blood circulation, while the latter supplied high affinity to tumor cells (Figure 1a). Afterward, the GO nanocomposite was internalized into ADSCs to assemble ADSC/NGO for the high efficiency targeting of a breast tumor through blood circulation, with less effect from the MPS attributed to the active immune evasion ability of live cells. Subsequently, first-stage NIR radiation was utilized to disrupt the ADSCs for GO-PEG-FA release, and the tumor cells efficiently entrapped the nanocomposites as a result of the high expression of FA receptors on the cell surface. After this, the heat generated by secondary-stage NIR radiation could destroy the malignant cells and shrink the tumor, and the cascade process could be recycled until complete tumor ablation if necessary (Figure 1b). We attempted to validate this ADSC-based tumor-targeting system for highly efficient GO delivery combined with two-stage NIR radiation for superior tumor ablation to winnow the ADSC essence to its dregs by employing the tumor-tropism advantage and eliminating the malignant transformation.

Materials and Methods
Ethics Statement
All the procedures including animal studies were approved by Southern Medical University Institutional Review Board and the Nanfang Hospital Animal Ethics Committee and conducted in accordance with the ethical standards of the National Health and Medical Research Council (China).

Materials

Polyethylene glycol methyl ether acrylate (PEG, Mn = 480 g/mol), dimethylformamide (DMF, Mn = 73.09 g/mol), 2-(dodecylthiocarbonothioylthio)-2-methylpropionic acid (DMP, Mn = 364.63 g/mol), ethylenediamine (Mn = 60.1 g/mol), folic acid (Mn = 441.4 g/mol), dichloromethane (DCM, Mn = 384.93 g/mol), N-(3-Dimethylaminopropyl)-N'-ethylcarbodiimide hydrochloride (EDC, Mn = 191.7 g/mol), and N-Hydroxysuccinimide (NHS, Mn = 115.09 g/mol) were purchased from Sigma-Aldrich (MO, USA) and used as received. Multiple-layer GO was purchased from Tanfeng Co., Ltd. (Zhejiang, China). Dulbecco's modified Eagle's medium (DMEM; high glucose), 1% penicillin/streptomycin, and fetal bovine serum (FBS) were purchased from Thermo Fisher Scientific (Waltham, MA, USA).

Synthesis of GO-PEG-FA

PEG-raft-COOH was synthesized through RAFT polymerization; briefly, PEG (2 g, 4.17 mmol), DMP (50 mg, 0.11 mmol), and DMF (6 mL) were added to a round bottom flask equipped with a magnetic stirring bar. The mixture was then immersed in an oil bath (80 °C) for 5 h after being deoxygenated with nitrogen. Then, the solution was cooled, the solvent was evaporated in a vacuum chamber, and the compound was dissolved in DCM after cold diethyl ether was used to precipitate the final yellow viscous product.

GO was dispersed by probe ultrasonication at a concentration of 1 mg/mL. Then, ethylenediamine (50 mg, 0.83 mmol), excess EDC (0.05 mmol), and NHS (0.04 mmol) were added to the dispersion, and the reaction was allowed to continue for 72 h with vigorous stirring. Afterward, the mixture was dialyzed with dialysis tubing (7 kDa) against distilled water for 48 h, followed by lyophilization to obtain the GO-NH$_2$ product.

The as-obtained GO-NH$_2$ was completely dispersed in distilled water (2 mg/mL), and excess PEG-raft-COOH (at a ratio of 1:4), EDC, and NHS were added and reacted for 72 h to coat PEG on the GO surface (GO-PEG), which was further dialyzed and lyophilized. FA was added to the GO-PEG solution after EDC and NHS crosslinking, and the final GO-PEG-FA product was collected and stored at 4 °C.

Characterization of GO and the GO-PEG-FA Nanocomposite

The chemical structures of the GO, GO-PEG, and GO-PEG-FA samples were analyzed using Fourier transform infrared (FT-IR) spectroscopy on a Nicolet iS10 FT-IR spectrophotometer (Thermo Fisher Scientific Inc., MA, USA). The carbon structures of the GO and GO-PEG-FA samples were studied by micro-Raman spectroscopy (WiTech alpha300R, Germany) operating at 532 nm wavelength at room temperature. The morphology of the GO-PEG-FA was further studied using scanning electron microscopy (SEM) (Tescan MIRA LMS, Czekh). In addition, the surface topography and height profile distribution of the graphene sheets were studied by using atomic force microscopy (AFM, Digital Instruments NanoScope V) in tapping mode. The ultraviolet-visible-near infrared (UV-Vis-NIR) absorption spectra of the GO and GO-PEG-FA at the same concentration of 100 µg/mL were obtained at room temperature using a Bechman DU 640 spectrophotometer (LabX Co., Ltd. ON, Canada).

Cell Preparation and Identification

ADSCs were harvested from the lipoaspirates of individuals who signed informed consent and underwent liposuction procedures, all the procedures were approved by the Southern Medical University Institutional Review Board and followed the declaration of Helsinki. In brief, blood cell residues and tissue debris were thoroughly removed from the lipoaspirate by washing with PBS and centrifugation at 800 g for 5 min at 25 °C, after which the lipoaspirate was digested using 0.075% type I collagenase at 37 °C for 45 min under slow agitation. The digested lipoaspirate was then centrifuged, and the resultant cell pellets were resuspended in complete medium (DMEM containing 1% penicillin/streptomycin and 10% FBS) and seeded in 25 cm^2 flasks. The MCF-7 breast cancer cell line was purchased from the Research Laboratory Collaboration Alliance of Nan Fang Hospital (Guangzhou, China). To determine the multi-lineage differentiation potential of the ADSCs, cells were cultured in adipogenic, osteogenic, and chondrogenic media according to a previous study.[36] The adipogenic, osteogenic, and chondrogenic differentiations of the ADSCs were evaluated by staining with Oil Red O, Alizarin red, and Alcian blue, respectively.

974

DovePress

International Journal of Nanomedicine 2023:18

Measurement of Cellular Uptake of the GO-PEG-FA Nanocomposite

A cellular uptake assay was conducted to test the GO-PEG-FA uptake by ADSCs. First, 4×10^4 ADSCs were collected and seeded in confocal culture dishes supplemented with complete medium. After 24 h, the culture medium was replaced with a fresh complete medium (0.5 mL) containing 5, 10, 50, 100, 300, or 500 µg/mL GO-PEG-FA conjugated with Rhodamine B. After another 24 h of culture, the culture medium was discarded, and the cells were treated with phosphate-buffered saline (PBS) to remove the unloaded GO-PEG-FA. The cellular uptake of GO-PEG-FA was determined through the observation and quantification of the fluorescent signals in cells using a confocal microscope (LSM980, Carl Zeiss, Germany).

Cellular Viability and in vitro Photothermal Treatment

The cellular viability of the GO-PEG-FA-laden cells with or without radiation treatment was evaluated using the cell counting Kit-8 (CCK-8) assay. ADSCs were seeded in 96-well plates at a density of 5000 cells/well. After culturing for 24 h, the medium in the well was changed to 0.5 mL DMEM medium containing GO-PEG-FA. The cells treated with DMEM alone served as controls. The wells were then irradiated with an 808 nm laser (2 W/cm^2) for 0 s, 1 min, and 5 min. The cellular viability was assayed by adding 20 µL of CCK-8 solution to each well. The absorbance was measured at 450 nm using a microplate reader, and the cell viability was evaluated based on the OD values. The cellular viability was calculated using the following formula: cellular viability rate = ODtreat-ODblank/ODcontrol-ODblank × 100%. TMaximal temperature thermographic images of cells laden with or without GO-PEG-FA were collected using an infrared thermal imaging camera (Fluke, VT04A, USA).

In vitro Migration and Co-Culture Assay

The migration ability of the ADSCs was assessed using transwell chambers with 8 µm pores (Corning Costar). First, 100 µL of the complete medium containing 3×10^4 ADSCs was seeded into each of the upper chambers. Each lower chamber contained 600 µL of DMEM with and without 3×10^4 MCF cells. After 24 h of culture, the cells on the upper surface were carefully removed with a cotton swab, and the cells adhering to the bottom surface were stained with DAPI. The number of ADSCs that migrated to the bottom surface was observed and photographed using a fluorescence microscope (Nikon). A co-culture assay was conducted to track the interaction between the GO-PEG-FA-laden ADSCs and MCF-7 cells in vitro. Briefly, GO-PEG-FA adsorbed Rhodamine B physically on the surface to label with red fluorescence, and the MCF-7 cells were labeled with green fluorescence using Vybrant® DiO Cell-Labeling Solution (Invitrogen; Thermo Fisher Scientific) according to the manufacturer's protocol. The same amounts (4×10^4) of GO-PEG-FA-laden ADSCs and MCF-7 cells were mixed uniformly in the culture medium and seeded in Matrigel (Growth-factor-reduced, 356230, BD Biosciences, NJ, USA) to fabricate a three-dimensional co-culture system. The cellular interactions between the GO-PEG-FA-laden ADSCs and MCF-7 cells were observed continuously using a confocal microscope for 96 h. Following fixation, dehydration, and embedding in resin, the microstructure after the endocytosis of this nanocomposite was observed using TEM (HT7800, HITACHI, Japan).

Tumor-Bearing Mice Preparation

BALB/c nude mice (female, 4–5 weeks; 13–15 g) were purchased from the Laboratory Animal Center of Nanfang Hospital, Southern Medical University and housed at 25 ± 2 °C and 55% humidity in a pathogen-free animal facility. Breast tumor-bearing models were established according to a previously described protocol.[37] In brief, 0.5 mL of PBS containing 2×10^6 MCF-7 cells were subcutaneously injected into each side of the groin fat pad of the mouse. The mice were used after the tumor volume reached approximately 100 mm^3.

GO-PEG-FA-Laden ADSCs Homing to Tumors and in vivo Photothermal Treatment

Cell labeling was performed according to the manufacturer's protocol to trace the ADSCs in vivo. In brief, 5×10^5 ADSCs in 1 mL of PBS were treated with 5 µL of DiI labeling solution (Invitrogen; Thermo Fisher Scientific, Inc. USA) and cultured at 37 °C for 15 min. After labeling, the cells were seeded in 25 cm^2 flasks. After incubation for 24 h, the medium was changed to DMEM containing 500 µg/mL GO-PEG-FA and incubated for 24 h to achieve double-stained GO-PEG-FA-laden ADSCs.

Then, the GO-PEG-FA-laden ADSCs were harvested, washed with PBS, and injected into the tail veins of the tumor-bearing mice. The tumor-bearing mice were randomized into four groups and treated with either 1) PBS (0.5 mL), 2) ADSCs (5×10^5 in 0.5 mL PBS), 3)GO-PEG-FA (0.5 mL, 500 μg/mL), or 4) GO-PEG-FA-laden ADSCs (5×10^5 in 0.5 mL PBS) by tail intravenous injection. Four weeks after the treatment, the bioluminescence imaging of the mice was used to trace the ADSCs using an in vivo fluorescence imaging system (Carestream Health, Inc., Rochester, NY, USA). For the photo-thermal treatment, the mice were assigned randomly and treated with NIR radiation at the tumor site using a photodynamic apparatus (808 nm, 4 W cm^{-2}, 10 min). The maximum temperature and infrared thermographic images of the tumor site were recorded using an infrared thermal imaging camera. The tumor sizes were measured every 4 days for 32 consecutive days, and the body weight of each mouse was recorded weekly. Approximate tumor volumes were calculated using the following formula: tumor volume = length × width^2/2.

Histological Analysis and Fluorescence Detection

The mice were euthanized 4 weeks after the tail intravenous injection by cervical dislocation after being deeply anesthetized by an intraperitoneal injection of pentobarbital (40 mg/kg). The tumors and four key organs (heart, liver, kidney, and lung) were excised, embedded with optimal cutting temperature compound (OCT), and frozen. Hematoxylin and eosin (H&E) staining was used to evaluate the histological structures of the frozen samples under a light microscope. For the detection of the GO-PEG-FA-laden ADSCs in the tumors, the frozen samples were sliced, and the sections were observed under a fluorescent microscope to observe both the GO and ADSC fluorescence signals. The nuclei were counterstained with 4',6-diamidino-2-phenylindole (DAPI).

Statistical Analysis

The data are presented as the mean values ± SD of multiple determinations. Multiple comparisons of the migrated ADSCs were performed using a one-way analysis of variance, and a least significant difference post hoc analysis was performed to ascertain the significance among the groups. The statistical significance was set at $P < 0.05$.

Results and Discussions
Synthesis and Characterization of GO-PEG-FA

In this study, GO nanocomposites were coated with PEG-raft-COOH and decorated with FA, as described in Figure 1a. The GO nanostructure was first functionalized with ethylenediamine to convert the carboxyl group into an amino group, after which GO-NH$_2$ was coated with PEG-raft-COOH via EDC conjugation to improve the hydrophilicity and cytocompatibility, and FA was finally decorated on the as-synthesized GO-PEG for exclusive tumor cell targetability. The chemical structures of the GO, PEG, GO-PEG, and GO-PEG-FA were confirmed by the FTIR spectra shown in Figure 2a. GO exhibited a broad stretching O–H bond at 3100–3400 cm^{-1}, indicating the presence of hydroxyl groups, as well as water molecules. The peaks at approximately 1730 and 1020 cm^{-1} correspond to the stretching vibrations of the C = O band on the –COOH and C–O (epoxy) groups in GO, respectively. The PEG-related bands at 1654 and 2840 cm^{-1} were attributed to the stretching vibrations of C = O and C–H. The major peaks in PEG and GO were preserved in the GO-PEG compound, with a minor location shift and relative transmission change. After the FA grafting, a couple of new features appeared. The peaks at 3300–3400 cm^{-1} correspond to the N-H group, and the signal at 1715 cm^{-1} indicates that the amide group of the FA was attached to the nanosheet. These signatures of the functional groups in the GO, PEG, and FA confirmed the successful conjugation of GO-PEG-FA. Raman spectroscopy was applied to study the carbon structure of GO and GO-PEG-FA sheets, as shown in Figure 2b, Classical D-band (~1346 cm^{-1}), G-band (~1576 cm^{-1}) and 2D-band (~2696 cm^{-1}) were observed in GO and GO-PEG-FA sheets. The representative SEM images in Figure 2c (left) shown a loosely stacked and typical wrinkled surface structure for GO, after carrying PEG and FA, the edge of GO-PEG-GA is obviously passivated by the decoration. Figure 2c (right) shown AFM images of the GO and GO-PEG-FA sheets, suggested that the thickness of GO-PEG-FA (~1.03 nm) is significantly higher than that of GO (~2.2 nm). The stabilities of the GO and GO-PEG-FA were compared in distilled water, phosphate buffer saline (PBS, 0.1 M), and culture medium at the same concentration (100 μg/mL) after complete ultrasonication. As shown in Figure 2d, after the ultrasonic
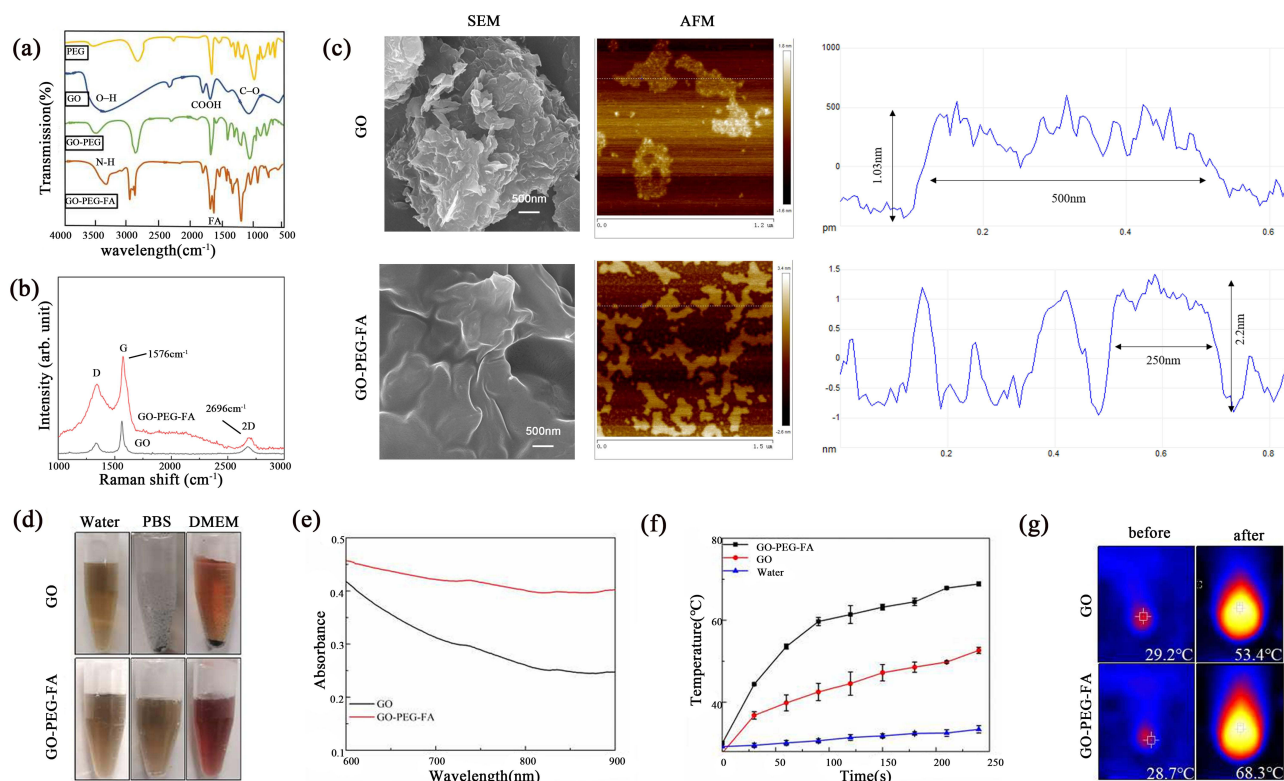
Figure 2 (**a**) FTIR spectra of PEG, GO, GO-PEG, and GO-PEG-FA. (**b**) Raman spectra of GO and GO-PEG-FA. (**c**) Left: SEM images of the GO and GO-PEG-FA. Middle: AFM images of GO and GO-PEG-FA. Right: Size of GO and GO-PEG-FA (**d**) GO and GO-PEG-FA. (**d**) Nanocomposites dispersion in distilled water, PBS buffer, and cell culture medium after 24 h. (**e**) UV-Vis-NIR absorption spectra of GO and GO-PEG-FA. (**f**) Assessment of temperature elevation of GO, GO-PEG-FA, and water under NIR radiation (808 nm, 4W cm^{-2}) for 240 s. (**g**) Temperature change of GO and GO-PEG-FA after the same period of radiation.
Abbreviations: FTIR, Fourier Transform infrared spectroscopy; GO, Graphene oxide; PEG, poly-ethylene glycol; FA, folic acid; SEM, scanning electron microscopy; AFM, Atomic Force Microscope; PBS, phosphate buffered solution; UV-Vis-NIR, ultraviolet-visible-near infrared.

treatment, GO only maintained a homogeneous state in an aqueous solution and could not maintain a good dispersion state in a physical solution such as PBS and culture media, resulting in repaid precipitation induced by the equilibrium disruption of the electrostatic effect. In contrast, the GO-PEG-FA exhibited excellent biostability in all the media, which was attributed to the hydrophilic PEG modification and strongly implied enhanced cytocompatibility, as well as photothermal therapy potential.[9,38] The UV-Vis-NIR absorption spectra of GO and GO-PEG-FA (at a concentration of 100 µg/mL) were obtained to directly demonstrate the photon absorption capability (Figure 2e). Significantly increased intensities in both the visible and NIR ranges (600–900 nm) after the PEG and FA decoration were revealed, and the enhancement in the intensity at 808 nm reached 55.9%, which may be attributed to the chemical modification of the PEG and FA groups on GO. Subsequently, the photothermal effect on the heat generation of the GO and GO-PEG-FA solution with NIR (808 nm, 4 W cm^{-2}) radiation for 240 s was assessed (Figure 2f). GO-PEG-FA showed significant temperature elevation from 29.2 to 68.3 °C, whereas GO only reached 53.4 °C from the initial 28.7 °C after the same period of radiation (Figure 2g). Consequently, the biostability and photothermal effect of GO were effectively modulated by the chemical conjugation of PEG and FA.

Multilineage Differentiation of ADSCs, Cellular Uptake, and Cytotoxicity Investigation

The ADSCs isolated from the donated fat grew well in vitro and were subjected to adipogenic, osteogenic, and chondrogenic induction to verify their multipotent differentiation ability. After the induction, the cells were found to contain matrix mineralization, cartilage-specific proteoglycans, and lipid droplets, and were stained positively for Alizarin Red S (Figure 3a), Alcian Blue (Figure 3b), and Oil Red O (Figure 3c).

The cellular uptake efficiency is an important factor in the development of a cell-nanocomposite system. The cellular uptake of GO-PEG-FA was evaluated by fluorescence microscopy and is shown in Figure 4a. Both the ADSCs and MCF-7
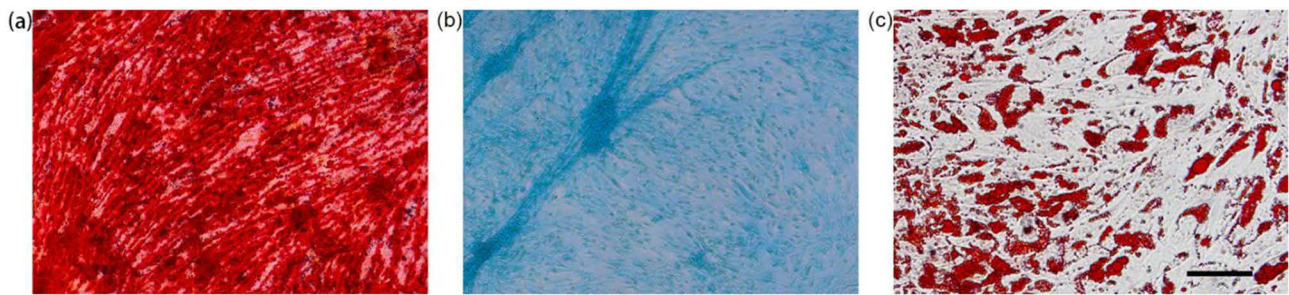
Figure 3 (**a**) Osteogenic, (**b**) Chondrogenic and (**c**) Adipogenic differentiation of ADSCs isolated from donated fat. Scale bar = 100 μm.
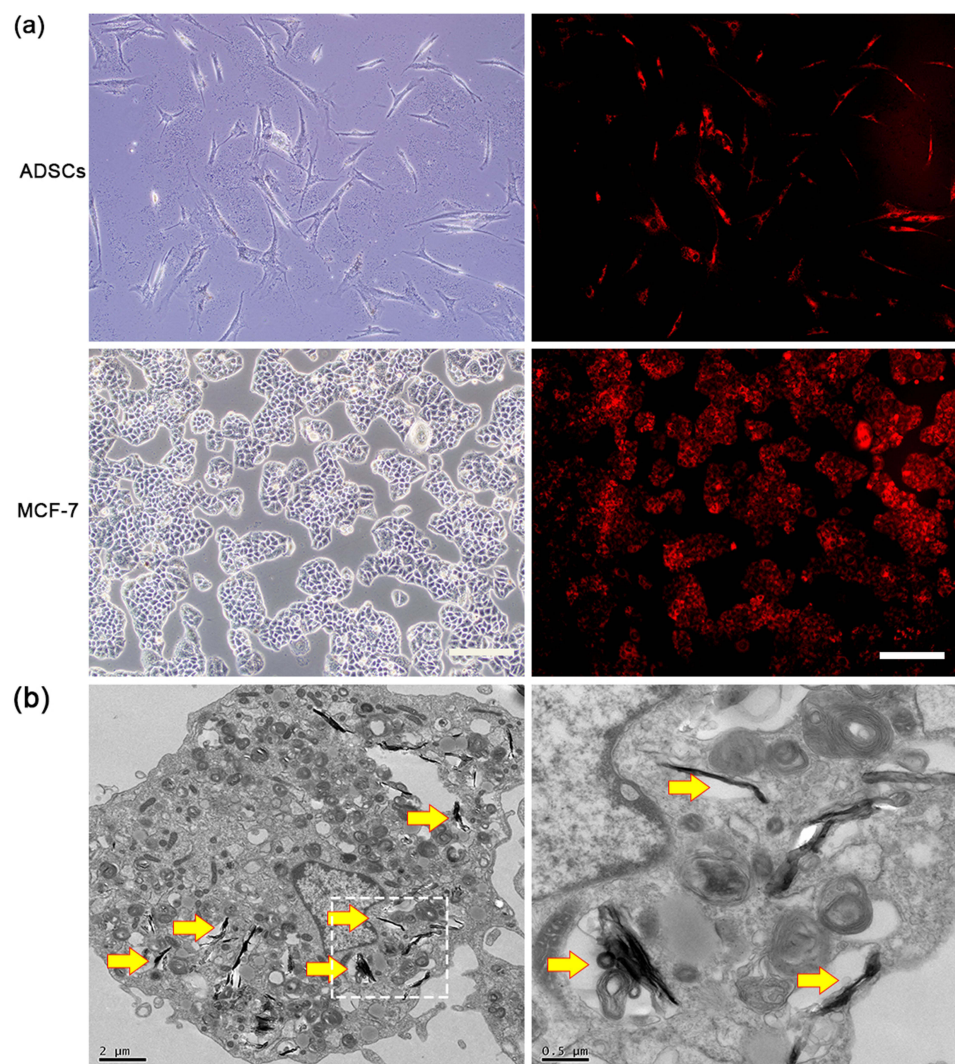**Abbreviation**: ADSCs, Adipose-derived stem cells.

Figure 4 Cellular uptake of GO-PEG-FA. (**a**) Cellular uptake of GO-PEG-FA in ADSCs and MCF-7 cells under light and fluorescence microscope. (**b**) GO-PEG-FA aggregates (yellow arrows) in ADSCs validated by TEM images in different magnifications. The picture on the right is the picture in the white dotted line box on the left after being magnified by 4 times. White scale bar = 200 μm.
Abbreviations: GO, Graphene oxide; PEG, poly-ethylene glycol; FA, folic acid; ADSCs, Adipose-derived stem cells; TEM, Transmission Electron Microscope.
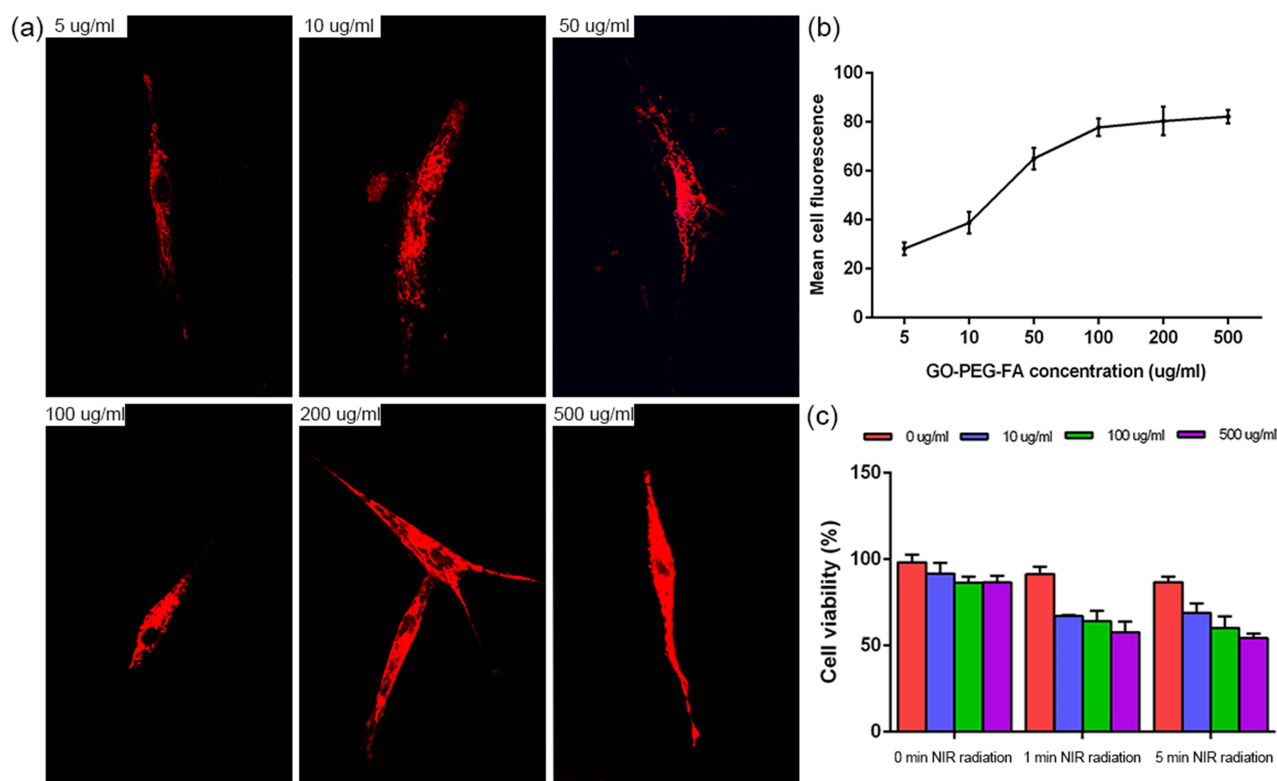
Figure 5 (**a**) fluorescence images of ADSCs treated GO-PEG-FA of different concentrations. (**b**) Quantification of mean cell fluorescence. (**c**) Cell viability measurement.
Abbreviations: ADSCs, Adipose-derived stem cells; GO, Graphene oxide; PEG, poly-ethylene glycol; FA, folic acid.

cells incubated with Rhodamine B-labeled GO-PEG-FA exhibited red fluorescence throughout the cells, with an unaltered cell morphology, indicating the entrance of a substantial amount of GO into the cells. The GO-PEG-FA within the cytoplasm was observed using TEM. Figure 4b shows the GO-PEG-FA aggregates that were identified in the membrane-bound structures inside the cells. The mean cell fluorescence density of the ADSCs increased gradually with an increase in their GO-PEG-FA uptake concentration from 5 to 100 μg/mL and remained stable with a further increase in the GO-PEG-FA uptake concentration from 100 to 500 μg/mL (Figure 5a and b). This indicates that 100 μg/mL was the maximum uptake concentration of GO-PEG-FA for the ADSCs.

Nanomaterials must have sufficient biocompatibility to ensure that cellular functions are not impaired in cell delivery systems. To assess the cytotoxicity of GO-PEG-FA on the ADSCs with or without the NIR radiation treatment, the cell viability was determined. As shown in Figure 5, GO-PEG-FA alone appeared to be nontoxic to the ADSCs at the tested concentrations, while the NIR-radiated GO-PEG-FA caused a reduction in the cell viability with a prolonged exposure time and increased the GO-PEG-FA concentration. The results demonstrated that GO-PEG-FA alone did not affect the cell viability, but the hyperthermia effect induced by the NIR-radiated GO caused a reduction of up to 32% in the cell viability as compared to the untreated group (Figure 5c). Moreover, the NIR radiation had nearly no effect on the viability of the cells without GO-PEG-FA loading, indicating that the energy produced by the NIR radiation did not damage the cells.

GO-PEG-FA-Laden ADSCs Exhibit Higher Selective Tropism and Accumulation in Tumors

Transwell migration assays were used to explore the tropism of the ADSCs in the MCF-7 cells. The results revealed that a significantly larger number of ADSCs migrated to the bottom surface of the upper chambers as compared to the control group (Figure 6a). To investigate the cellular interactions between the GO-PEG-FA-laden ADSCs and MCF-7 cells, a co-culture assay was conducted in vitro. During the co-culture, we found that the GO-PEG-FA-laden ADSCs migrated toward the MCF-7 cells and ultimately adhered to the contact (Figure 6b).
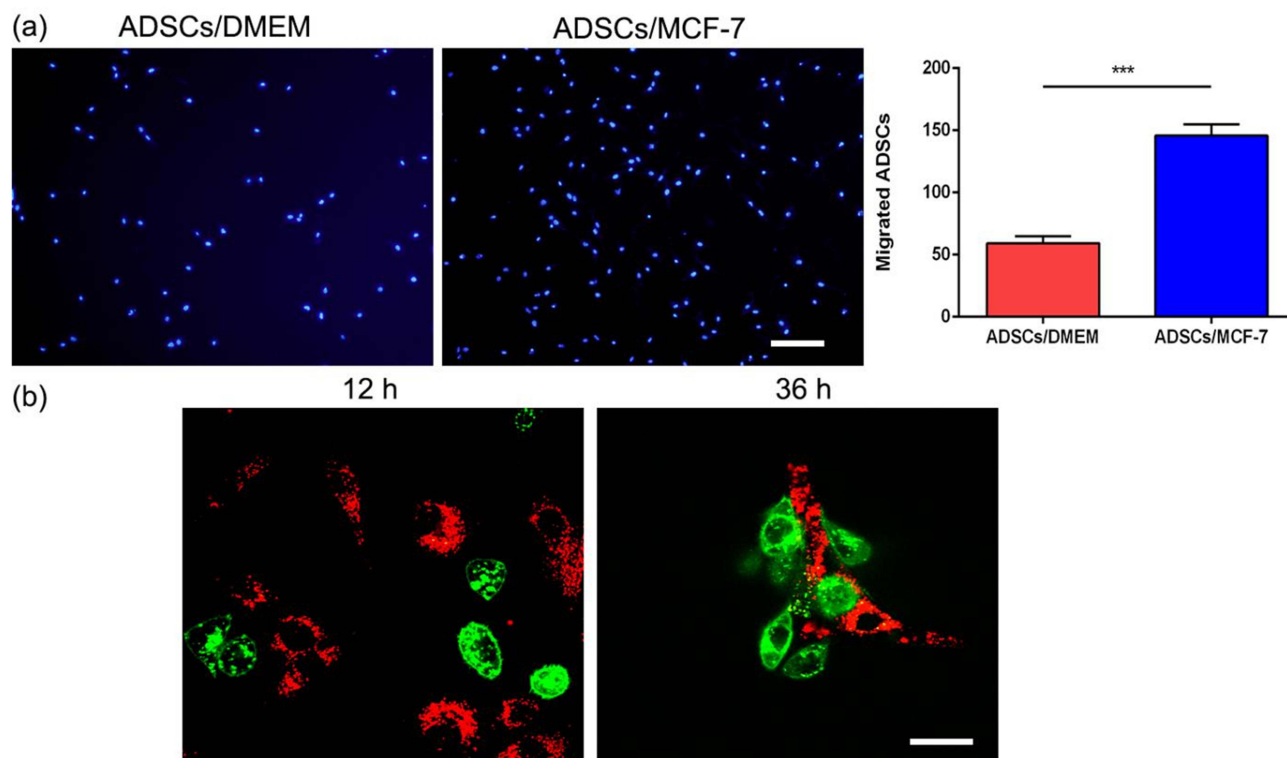
Figure 6 (**a**) Transwell migration assay, Migration of ADSCs treated with DMEM and MCF-7 respectively. (**b**) Interaction between ADSCs and MCF-7 in vitro, MCF-7 cells in green and ADSCs loaded with GO-PEG-FA in red. Scale bar=100 μm. ***p<0.001.
Abbreviations: ADSCs, Adipose-derived stem cells; DEME, dulbecco's modified eagle medium; GO, Graphene oxide; PEG, poly-ethylene glycol; FA, folic acid.

We next investigated the migration of the ADSCs to the MCF-7 cells in vivo. The migration of the GO-PEG-FA-laden ADSCs in the tumor-bearing mice was monitored using an in vivo fluorescence imaging system. Representative images showed that the GO-PEG-FA-laden ADSCs was first found in the lung and subsequently localized to the liver, but the fluorescence signal in the liver reduced slightly 7 days post-injection, and a weak fluorescence activity was observed at the tumor sites. By 14 days post-injection, the fluorescence signal was greatly reduced in the liver, while a high level of fluorescence activity was visible at the tumor sites. Notably, at 32 days post-injection, only the tumors displayed fluorescence signals, and all the organs were devoid of the fluorescence signal (Figure 7a). These results preliminarily demonstrated the systemic delivery of GO-PEG-FA into the tumors via the ADSC vehicles. Fluorescent microscopic observation was performed on the tumor sections to further evaluate the retention of the GO-PEG-FA-laden ADSCs in the tumors at day 32. The sections showed that both red and green fluorescence signals were observed in the tumors, with the two fluorescence signals largely coinciding (Figure 7b). The results demonstrated that the systemic-delivered ADSCs carrying GO-PEG-FA could deeply infiltrate and remain in the tumors in this study. The tumor-homing ability of the MSCs has been verified in many experimental settings and in preclinical studies.[39,40] MSC migration to tumor sites has been proven to be mediated by various chemoattractants such as stromal cell-derived factor 1, monocyte chemotactic protein-1, and the macrophage inflammatory protein secreted by hypoxic tumor cells.[41,42] Previous study showed non-covalent polymer or RGD coating GO nanomaterials exhibit remarkably prolonged blood circulation and efficient tumor passive accumulation.[43,44] However, the uptake rate of nanomaterials by RES organs, including liver and spleen, mainly depends on the size of the sheets. In this experiment, different from the two-compartment model of drug metabolism, the biodistribution of graphene sheets mainly depends on the in vivo distribution behavior of ADSCs, which takes much longer than the previous half-life of graphene. The in vivo migration of ADSCs was consistent with the results of a previous study that showed that MSCs systemically delivered to tumor-bearing animals initially resided in the lungs, then migrated to the liver, and finally remained in the tumor sites.[32] This indicates that the successful migration of the GO-PEG-FA-laden ADSCs to tumors may rely on the tumor tropism of the ADSCs.
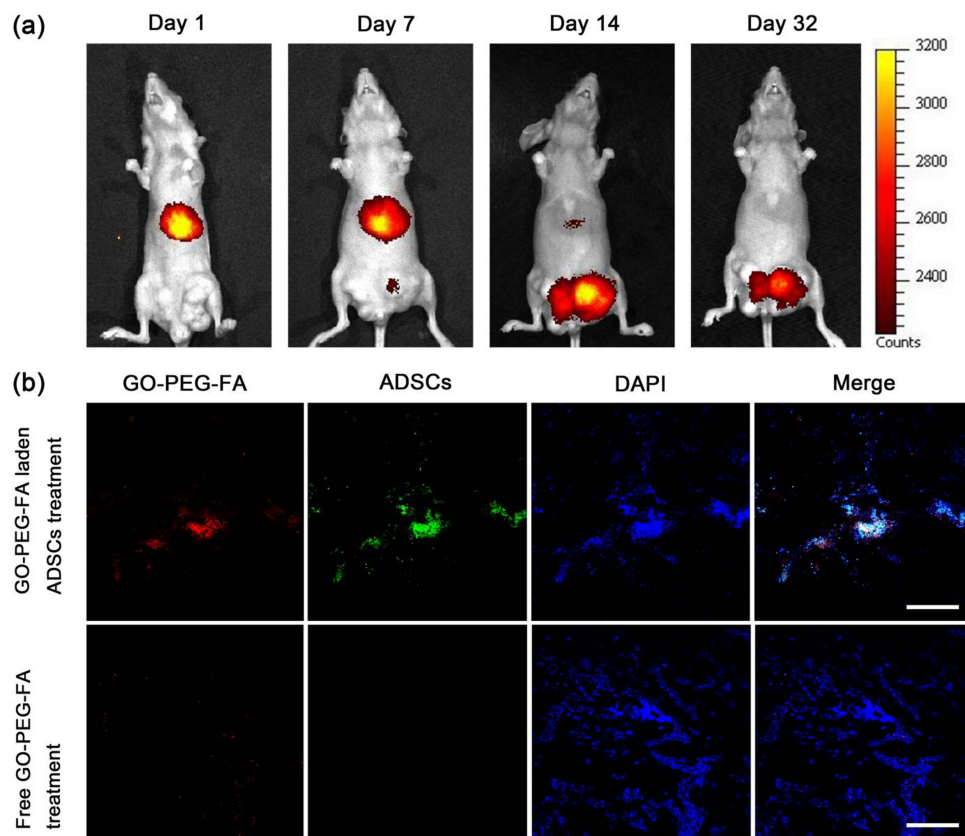
Figure 7 (**a**) Tracing of GO-PEG-FA laden ADSCs in tumor-bearing mice after tail veins injection via a bioluminescence imaging system. (**b**) Fluorescent microscopic detection of GO-PEG-FA laden ADSCs and free GO-PEG-FA retention at day 32 after intravenous injection. Scale bar=100 μm.
Abbreviations: GO, Graphene oxide; PEG, poly-ethylene glycol; FA, folic acid; ADSCs, Adipose-derived stem cells.

GO-PEG-FA-Laden ADSCs Exhibit Excellent Photothermal Efficacy Both in vitro and in vivo

The results of the in vitro photothermal assay are shown in Figure 8. Under 808 nm NIR radiation, the maximum temperature of the GO-PEG-FA-laden ADSCs increased from 38.2 to 39.5 °C during the first minute and reached 42.6 °C after 8 min. Nevertheless, the maximum temperature of the ADSCs without GO-PEG-FA increased from 31.2 to 31.7 °C during the first minute and remained almost stable during the following treatment period (Figure 8). However, We have not observed the process of ADSC releasing GO-PEG-FA under irradiation. This is a flaw in our experiment.
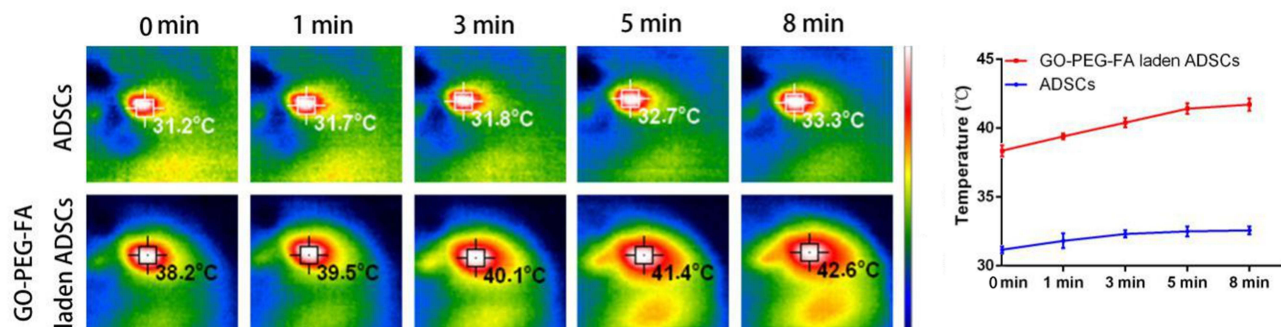

Figure 8 In vitro photothermal assay. Temperature trends of ADSCs and ADSCs loaded with GO-PEG-FA after NIR radiation.
Abbreviations: ADSCs, Adipose-derived stem cells; GO, Graphene oxide; PEG, poly-ethylene glycol; FA, folic acid; NIR, near-infrared laser radiation.
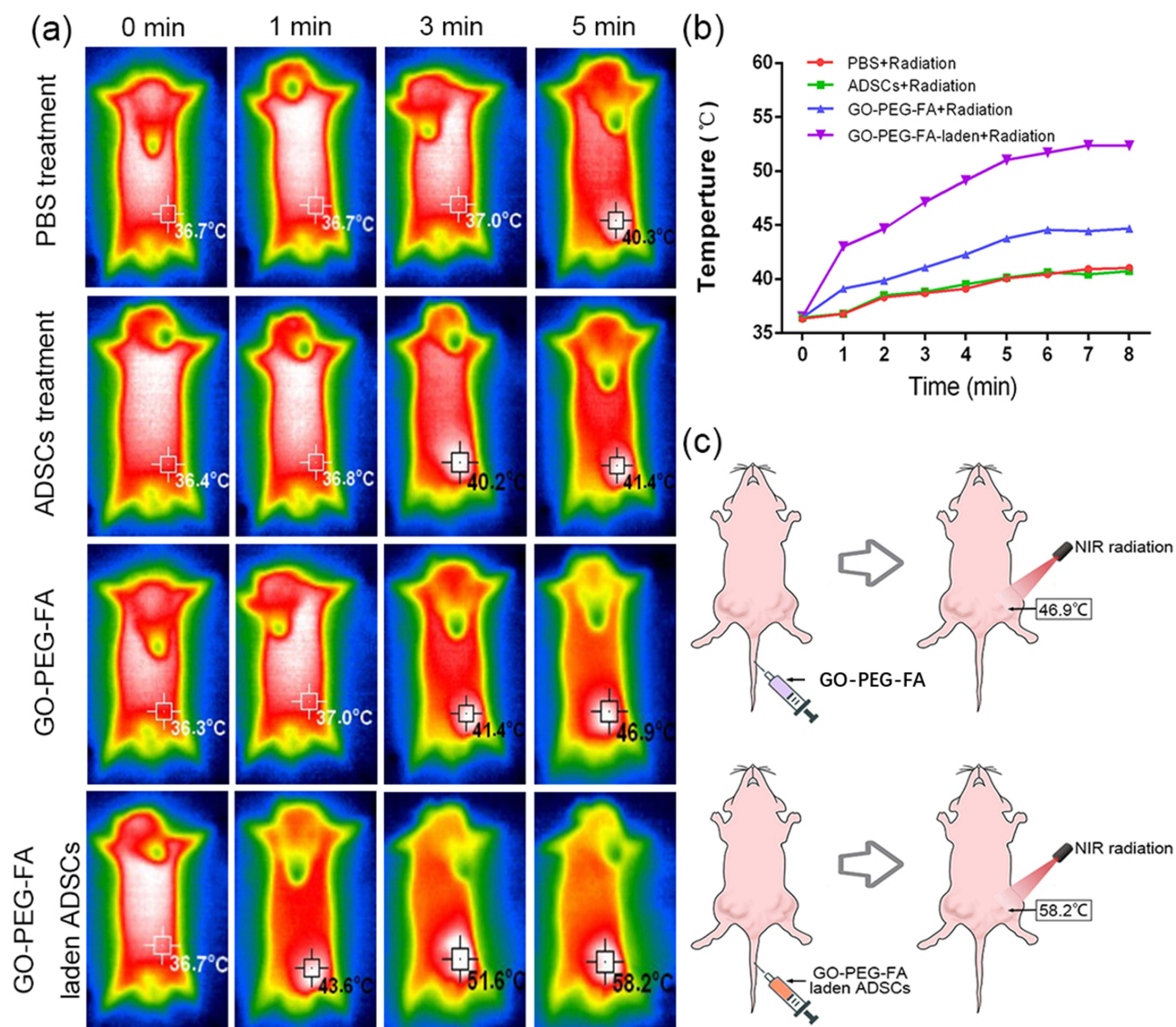
Figure 9 In vivo photothermal assay, (**a**) in vivo thermal images of the tumor site after treated with NIR radiation. (**b**) Temperature trends of tumor sites in mice in each group after NIR radiation treatment. (**c**) The highest temperature reached at the tumor site after NIR radiation treatment in mice after injection of GO-PEG-FA or GO-PEG-FA-laden ADSCs via the rat tail vein.
Abbreviations: NIR, near-infrared laser radiation; GO, Graphene oxide; PEG, poly-ethylene glycol; FA, folic acid; ADSCs, Adipose-derived stem cells.

A similar trend was observed in the in vivo thermal images. The maximal temperature of the tumor treated with the GO-PEG-FA-laden ADSCs increased from 36.7 to 43.6 °C during the first minute and reached as high as 58.2 °C after 5 min. In contrast, the maximal temperature of the tumor in the ADSC-treated mice increased from 36.4 to 36.8 °C during the first minute and reached 41.4 °C after 5 min. In addition, the maximal temperature of the tumor in the free GO-PEG-FA-treated mice increased from 36.3 to 37 °C during the first minute and reached 46.9 °C after 5 min. These results indicated that the GO-PEG-FA-laden ADSCs exhibited excellent photothermal efficacy both in vitro and in vivo (Figure 9).

GO-PEG-FA-Laden ADSCs Exhibit Excellent Antitumor Effect in Mice

The antitumor effect of the GO-PEG-FA-laden ADSCs on tumor growth was evaluated in a breast tumor model using BALB/c nude mice. The mice were randomly intravenously injected with PBS, GO-PEG-FA, or the GO-PEG-FA-laden ADSCs. Each group was then treated with two-stage NIR radiation for an interval of 3 days at the tumor site using a power of 4 W cm^{-1} and a wavelength of 808 nm. The tumor specimens were subjected to H&E staining after 12 days of
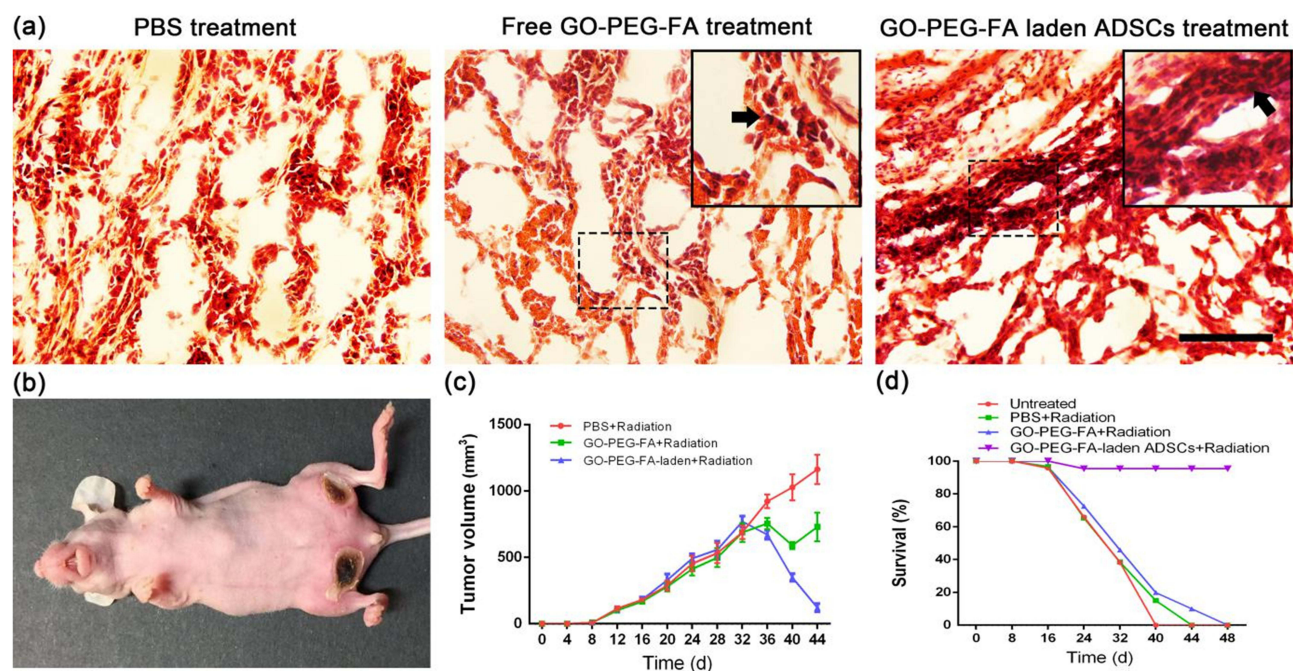
Figure 10 (**a**) H&E staining of the tumor tissue. Black arrows point out the GO aggregations. (**b**) Typical photographs of the mice treated with GO-PEG-FA laden ADSCs after the NIR treatment at day 44. (**c**) Tumors growth in the different groups at different time points after the treatments. (**d**) Survival rate in the different groups at different time points after the treatments.
Notes: The picture in the black solid line box is the enlarged picture in the black dotted line box. Scale bar=400 μm.
Abbreviations: H&E, hematoxylin-eosin staining; GO, Graphene oxide; PEG, poly-ethylene glycol; FA, folic acid; ADSCs, Adipose-derived stem cells.

the NIR radiation treatment (Figure 10a). The deformation of the nucleus was observed in the GO-PEG-FA-laden ADSC treatment group, and intact and plump tumor cell nuclei were observed in the PBS treatment group. The nuclei in the free GO-PEG-FA treatment group partially dwindled with irregular morphological changes. Furthermore, significantly larger aggregated black dots (black arrow), which represented the GO particles, were detected in the tumor sections of the mice treated with the GO-PEG-FA-laden ADSCs as compared to those treated with GO-PEG-FA.

The antitumor effect was further investigated after the NIR treatment in all three groups. All the radiated tumors in the mice treated with the GO-PEG-FA-laden ADSCs disappeared 2 days after the NIR radiation treatment, leaving black scars at the tumor site, which fell off approximately 1 week later (Figure 10b), whereas the tumor volume in the GO-PEG-FA-treated mice remained stable over time. In the PBS-treated group, the tumors grew continuously, with the tumor volume increasing from 637 to approximately 981 mm^3 after 14 days, demonstrating that the NIR radiation itself did not affect the tumor development. A statistical analysis showed that the tumor volume in the GO-PEG-FA-laden ADSC-treated group was significantly smaller than those in the other two groups (p < 0.001 with PBS/ GO-PEG-FA-laden ADSCs, 0.026 with PBS/ GO-PEG-FA, and 0.001 with GO-PEG-FA/GO-PEG-FA-laden ADSCs) on day 44. In comparison to the PBS control group at day 44, a tumor inhibition of almost 88% was achieved in the cell-treated group, while an inhibition efficiency of only 32% was achieved in the GO-PEG-FA-treated group (Figure 10c). The results demonstrated the excellent anti-tumor efficiency of the combined application of GO-PEG-FA and ADSCs in comparison to that of free GO-PEG-FA.

GO-PEG-FA-Laden ADSCs Exhibit Favorable Biocompatibility in vivo

Yang et al found that nanographene sheets (NGS) showed a high tumor uptake rate in several xenograft tumor mouse models in vivo, while the accumulation of NGS in the reticuloendothelial system, including liver and spleen, were surprisingly low. The ultrahigh tumor accumulation of NGS could be due to the enhanced permeability and retention (EPR) effect in cancerous tumors with tortuous and leaky vasculatures, which tend to trap materials in the nanosize range. However, the high kidney uptake of NGS might indicate possible renal excretion of NGS with small sizes.[38] Fazaeli et al obtained similar results that the major activity of the nanostructure after 24 h post-injection was found in the blood and kidneys in addition to the tumor, suggested that the main route of excretion for the nanostructures is urinary
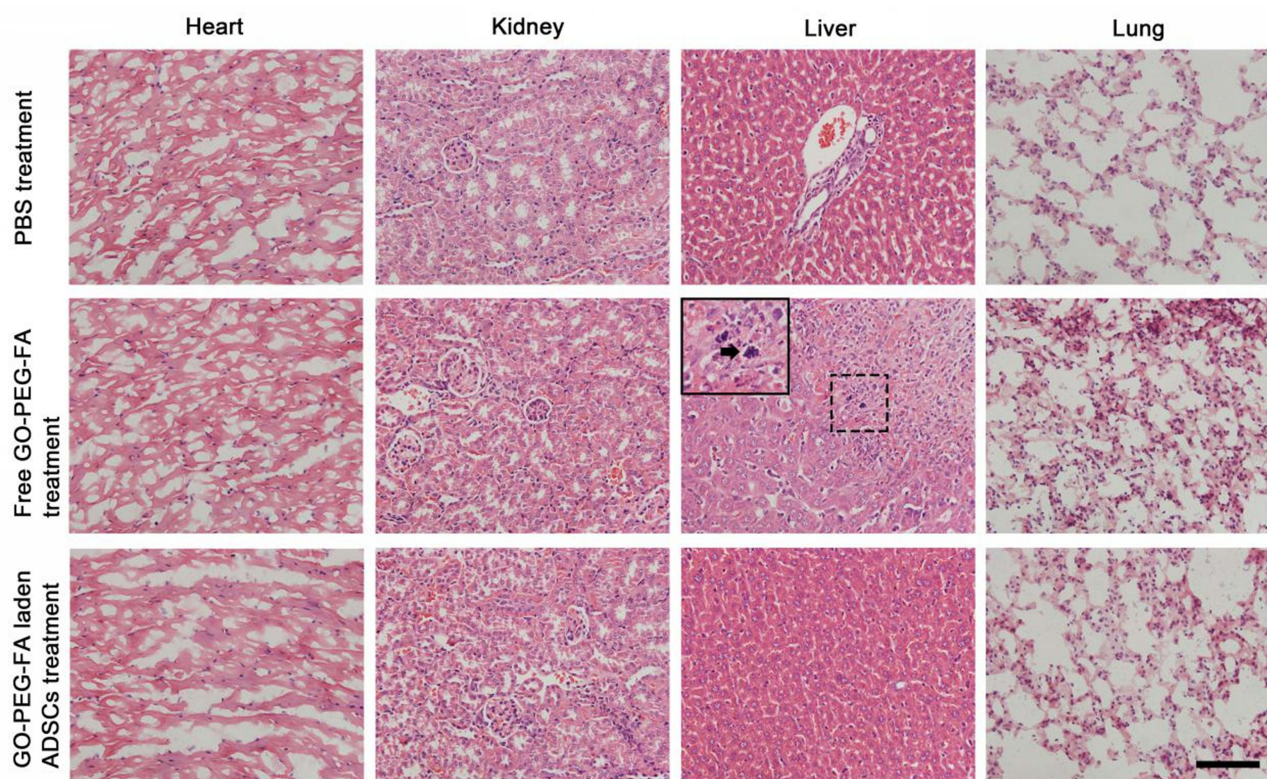
Figure 11 H&E stains of heart, kidney, liver, lung of mice in three groups, respectively. Black arrows point out the GO aggregations.
Notes: The picture in the black solid line box is the enlarged picture in the black dotted line box. Scale bar=400 µm.
Abbreviations: H&E, hematoxylin-eosin staining; GO, Graphene oxide.

tract.[45] To evaluate the toxicity and distribution of GO-PEG-FA in vivo, we observed the pathological changes in four important organs (heart, liver, kidney, and spleen) of the mice at day 44. The microscopic assessment indicated no obvious organ damage, tissue denaturation, or nanocomposite residue in the GO-PEG-FA- and PBS-treated mice (Figure 11). However, a small amount of black GO-PEG-FA was observed in the livers of the free GO-PEG-FA-treated mice (Figure 11, black arrow). Although obvious tissue damage was found only in the livers of the free GO-PEG-FA-treated mice, the potential damage of the remaining GO-PEG-FA to other living cells cannot be neglected as well. The longest survival was observed in the tumor-bearing mice treated with the GO-PEG-FA-laden ADSCs (Figure 10d). Unfortunately, most of the tumor-bearing mice treated with PBS died within 12 days after the NIR radiation treatment, and the treatment with free GO-PEG-FA showed no significant improvement in survival. These results demonstrated that the systematic administration of GO-PEG-FA had no obvious toxicity to the key organs and tumor-bearing mice. Nanomaterial-mediated PTT has been considered as a promising strategy for cancer therapy in recent years.[46–48] However, one of the greatest challenges in translating PTT into clinical use is the low efficiency of nanocomposites homing to the tumor site after intravenous injection. In this study, we used an ADSC-mediated nanomaterial-delivery system for PPT via intravenous injection in a mouse breast cancer model. The use of ADSCs to facilitate the GO-PEG-FA delivery could significantly increase the accumulation of GO-PEG-FA in tumors, without the observation of pathological variation or nanocomposite residue in the main organs, leading to enhanced tumor inhibition. The administration of free GO-PEG-FA showed a distribution of nanocomposites in the liver, resulting in minimized tumor inhibition rates. These findings suggest that the ADSCs could serve as a promising carrier for improving PTT efficiency by optimizing the intratumoral distribution of the nanomaterials.

Conclusion

In summary, we reported a stem cell-based anticancer system that used GO-PEG-FA-laden ADSCs for breast cancer therapy through NIR treatment in mice. The GO-PEG-FA showed minimal cytotoxicity and caused cell apoptosis after

NIR treatment in vitro. As compared to free GO-PEG-FA, the GO-PEG-FA-laden ADSCs exhibited higher selective tropism toward tumors after intravenous injection and led to enhanced tumor inhibition efficiency after the photothermal treatment in vivo. These findings highlight the advantages of combining cellular therapies and nanotechnology to achieve more effective antitumor results. However, further studies are needed to confirm the antitumor efficiency of this cell-mediated nanomaterial delivery system in clinical trials.

Acknowledgments

Disclosure

The authors declare that no known competing financial interests or personal relationships that could have appeared to influence the work reported in this paper.

References

1. Bray F, Ferlay J, Soerjomataram I, et al. Global cancer statistics 2018: GLOBOCAN estimates of incidence and mortality worldwide for 36 cancers in 185 countries. *CA Cancer J Clin*. 2018;68(6):394–424. doi:10.3322/caac.21492
2. Boughey JC, Attai DJ, Chen SL, et al. Contralateral Prophylactic Mastectomy (CPM) consensus statement from the American society of breast surgeons: data on CPM outcomes and risks. *Ann Surg Oncol*. 2016;23(10):3100–3105. doi:10.1245/s10434-016-5443-5
3. Yin T, Liu J, Zhao Z, et al. Redox sensitive hyaluronic acid-decorated graphene oxide for photothermally controlled tumor-cytoplasm-selective rapid drug delivery. *Adv Funct Mater*. 2017;27(14):1604620. doi:10.1002/adfm.201604620
4. Babavalian A, Tekie FSM, Ayazi H, et al. Reduced polydopamine coated graphene for delivery of Hset1 antisense as A photothermal and gene therapy of breast cancer. *J Drug Deliv Sci Technol*. 2022;73:103462. doi:10.1016/j.jddst.2022.103462
5. Ayazi H, Akhavan O, Raoufi M, et al. Graphene aerogel nanoparticles for in-situ loading/pH sensitive releasing anticancer drugs. *Colloids Surf B Biointerfaces*. 2020;186:110712. doi:10.1016/j.colsurfb.2019.110712
6. Zhou M, Liu S, Jiang Y, et al. Doxorubicin-loaded single wall nanotube thermo-sensitive hydrogel for gastric cancer chemo-photothermal therapy. *Adv Funct Mater*. 2015;25(29):4730–4739. doi:10.1002/adfm.201501434
7. Xue J, Zhao Z, Zhang L, et al. Neutrophil-mediated anticancer drug delivery for suppression of postoperative malignant glioma recurrence. *Nat Nanotechnol*. 2017;12(7):692–700. doi:10.1038/nnano.2017.54
8. Shahbazi R, Ozpolat B, Ulubayram K. Oligonucleotide-based theranostic nanoparticles in cancer therapy. *Nanomedicine*. 2016;11(10):1287–1308. doi:10.2217/nnm-2016-0035
9. Chauhan G, Chopra V, Tyagi A, et al. "Gold nanoparticles composite-folic acid conjugated graphene oxide nanohybrids" for targeted chemo-thermal cancer ablation: in vitro screening and in vivo studies. *Eur J Pharm Sci*. 2017;96:351–361. doi:10.1016/j.ejps.2016.10.011
10. Kalluru P, Vankayala R, Chiang C-S, et al. Nano-graphene oxide-mediated In vivo fluorescence imaging and bimodal photodynamic and photothermal destruction of tumors. *Biomaterials*. 2016;95:1–10. doi:10.1016/j.biomaterials.2016.04.006
11. Sun B, Wu J, Cui S, et al. In situ synthesis of graphene oxide/gold nanorods theranostic hybrids for efficient tumor computed tomography imaging and photothermal therapy. *Nano res*. 2017;10(1):37–48. doi:10.1007/s12274-016-1264-x
12. Yu J, Lin Y, Yang L, et al. Improved anticancer photothermal therapy using the bystander effect enhanced by antiarrhythmic peptide conjugated dopamine-modified reduced graphene oxide nanocomposite. *Adv Healthc Mater*. 2017;6(2):1600804. doi:10.1002/adhm.201600804
13. Omidi M, Fathinia A, Farahani M, et al. Bio-applications of graphene composites: from bench to clinic. In: *Advanced 2D Materials*. John Wiley & Sons; 2016:433–471.
14. Akhavan O, Ghaderi E, Emamy H. Nontoxic concentrations of PEGylated graphene nanoribbons for selective cancer cell imaging and photothermal therapy. *J Mater Chem*. 2012;22(38):2626–2633. doi:10.1039/c2jm34330d
15. Markovic ZM, Harhaji-Trajkovic LM, Todorovic-Markovic BM, et al. In vitro comparison of the photothermal anticancer activity of graphene nanoparticles and carbon nanotubes. *Biomaterials*. 2011;32(4):1121–1129. doi:10.1016/j.biomaterials.2010.10.030
16. Hatamie S, Akhavan O, Sadrnezhaad SK, et al. Curcumin-reduced graphene oxide sheets and their effects on human breast cancer cells. *Mater Sci Eng C*. 2015;55:482–489. doi:10.1016/j.msec.2015.05.077
17. Ma N, Liu J, He W, et al. Folic acid-grafted bovine serum albumin decorated graphene oxide: an efficient drug carrier for targeted cancer therapy. *J Colloid Interface Sci*. 2017;490:598–607. doi:10.1016/j.jcis.2016.11.097
18. Hashemi M, Omidi M, Muralidharan B, et al. Evaluation of the photothermal properties of a reduced graphene oxide/arginine nanostructure for near-infrared absorption. *ACS Appl Mater Interfaces*. 2017;9(38):32607–32620. doi:10.1021/acsami.7b11291
19. Low PS, Henne WA, Doorneweerd DD. Discovery and development of folic-acid-based receptor targeting for imaging and therapy of cancer and inflammatory diseases. *Acc Chem Res*. 2008;41(1):120–129. doi:10.1021/ar7000815
20. Muntimadugu E, Kumar R, Saladi S, et al. CD44 targeted chemotherapy for co-eradication of breast cancer stem cells and cancer cells using polymeric nanoparticles of salinomycin and paclitaxel. *Colloids Surf B*. 2016;143:532–546. doi:10.1016/j.colsurfb.2016.03.075
21. Bu LL, Rao L, Yu GT, et al. Cancer stem cell-platelet hybrid membrane-coated magnetic nanoparticles for enhanced photothermal therapy of head and neck squamous cell carcinoma. *Adv Funct Mater*. 2019;29(10):1807733. doi:10.1002/adfm.201807733
22. Tsoi KM, MacParland SA, Ma XZ, et al. Mechanism of hard-nanomaterial clearance by the liver. *Nat Mater*. 2016;15(11):1212–1221. doi:10.1038/nmat4718

23. Li Z, Huang H, Tang S, et al. Small gold nanorods laden macrophages for enhanced tumor coverage in photothermal therapy. *Biomaterials*. 2016;74:144–154. doi:10.1016/j.biomaterials.2015.09.038

24. Chitu V, Yeung YG, Yu W, et al. Measurement of macrophage growth and differentiation. *Curr Protoc Immunol*. 2011;Chapter 14:14–20. doi:10.1002/0471142735.im1420s92

25. Toledano FN, Lupu-Haber Y, Bronshtein T, et al. Reconstructed stem cell nanoghosts: a natural tumor targeting platform. *Nano Lett*. 2013;13 (7):3248–3255. doi:10.1021/nl401376w

26. Kang S, Lee J, Ryu S, et al. Gold nanoparticle/graphene oxide hybrid sheets attached on mesenchymal stem cells for effective photothermal cancer therapy. *Chem Mater*. 2017;29(8):3461–3476. doi:10.1021/acs.chemmater.6b05164

27. Jeong JO, Han JW, Kim JM, et al. Malignant tumor formation after transplantation of short-term cultured bone marrow mesenchymal stem cells in experimental myocardial infarction and diabetic neuropathy. *Circ Res*. 2011;108(11):1340–1347. doi:10.1161/CIRCRESAHA.110.239848

28. Mizukami H, Yagihashi S. Exploring a new therapy for diabetic polyneuropathy - the application of stem cell transplantation. *Front Endocrinol*. 2014;5:45. doi:10.3389/fendo.2014.00045

29. Bergfeld SA, DeClerck YA. Bone marrow-derived mesenchymal stem cells and the tumor microenvironment. *Cancer Metastasis Rev*. 2010;29 (2):249–261. doi:10.1007/s10555-010-9222-7

30. Quante M, Tu SP, Tomita H, et al. Bone marrow-derived myofibroblasts contribute to the mesenchymal stem cell niche and promote tumor growth. *Cancer Cell*. 2011;19(2):257–272. doi:10.1016/j.ccr.2011.01.020

31. Zhao Q, Gregory CA, Lee RH, et al. MSCs derived from iPSCs with a modified protocol are tumor-tropic but have much less potential to promote tumors than bone marrow MSCs. *Proc Natl Acad Sci USA*. 2015;112(2):530–535. doi:10.1073/pnas.1423008112

32. Chen Y, He Y, Wang X, et al. Adipose-derived mesenchymal stem cells exhibit tumor tropism and promote tumorsphere formation of breast cancer cells. *Oncol Rep*. 2019;41(4):2126–2136. doi:10.3892/or.2019.7018

33. Peng Z, Dong Z, Chang Q, et al. Tissue engineering chamber promotes adipose tissue regeneration in adipose tissue engineering models through induced aseptic inflammation. *Tissue Eng Part C Methods*. 2014;20(11):875–885. doi:10.1089/ten.tec.2013.0431

34. Kern S, Eichler H, Stoeve J, et al. Comparative analysis of mesenchymal stem cells from bone marrow, umbilical cord blood, or adipose tissue. *Stem Cells*. 2006;24(5):1294–1301. doi:10.1634/stemcells.2005-0342

35. Strioga M, Viswanathan S, Darinskas A, et al. Same or not the same? Comparison of adipose tissue-derived versus bone marrow-derived mesenchymal stem and stromal cells. *Stem Cells Dev*. 2012;21(14):2724–2752. doi:10.1089/scd.2011.0722

36. Eterno V, Zambelli A, Pavesi L, et al. Adipose-derived Mesenchymal Stem Cells (ASCs) may favour breast cancer recurrence via HGF/c-Met signaling. *Oncotarget*. 2014;5(3):613–633. doi:10.18632/oncotarget.1359

37. Wang W, Zhong W, Yuan J, et al. Involvement of Wnt/beta-catenin signaling in the mesenchymal stem cells promote metastatic growth and chemoresistance of cholangiocarcinoma. *Oncotarget*. 2015;6(39):42276–42289. doi:10.18632/oncotarget.5514

38. Yang K, Zhang S, Zhang G, et al. Graphene in mice: ultrahigh in vivo tumor uptake and efficient photothermal therapy. *Nano Lett*. 2010;10 (9):3318–3323. doi:10.1021/nl100996u

39. Wu X, Hu J, Zhou L, et al. In vivo tracking of superparamagnetic iron oxide nanoparticle-labeled mesenchymal stem cell tropism to malignant gliomas using magnetic resonance imaging. Laboratory investigation. *J Neurosurg*. 2008;108(2):320–329. doi:10.3171/JNS/2008/108/2/0320

40. Kidd S, Spaeth E, Dembinski JL, et al. Direct evidence of mesenchymal stem cell tropism for tumor and wounding microenvironments using in vivo bioluminescent imaging. *Stem Cells*. 2009;27(10):2614–2623. doi:10.1002/stem.187

41. Dwyer RM, Potter-Beirne SM, Harrington KA, et al. Monocyte chemotactic protein-1 secreted by primary breast tumors stimulates migration of mesenchymal stem cells. *Clin Cancer Res*. 2007;13(17):5020–5027. doi:10.1158/1078-0432.CCR-07-0731

42. Menon LG, Picinich S, Koneru R, et al. Differential gene expression associated with migration of mesenchymal stem cells to conditioned medium from tumor cells or bone marrow cells. *Stem Cells*. 2007;25(2):520–528. doi:10.1634/stemcells.2006-0257

43. Yang K, Wan J, Zhang S, et al. The influence of surface chemistry and size of nanoscale graphene oxide on photothermal therapy of cancer using ultra-low laser power. *Biomaterials*. 2012;33(7):2206–2214. doi:10.1016/j.biomaterials.2011.11.064

44. Akhavan O, Ghaderi E. Graphene nanomesh promises extremely efficient in vivo photothermal therapy. *Small*. 2013;9(21):3593–3601. doi:10.1002/smll.201203106

45. Fazaeli Y, Akhavan O, Rahighi R, et al. In vivo SPECT imaging of tumors by 198,199Au-labeled graphene oxide nanostructures. *Mater Sci Eng C*. 2014;45:196–204. doi:10.1016/j.msec.2014.09.019

46. de Melo-Diogo D, Pais-Silva C, Dias DR, et al. Strategies to improve cancer photothermal therapy mediated by nanomaterials. *Adv Healthc Mater*. 2017;6(10):1700073. doi:10.1002/adhm.201700073

47. Choi WI, Kim J-Y, Kang C, et al. Tumor regression in vivo by photothermal therapy based on gold-nanorod-loaded, functional nanocarriers. *ACS Nano*. 2011;5(3):1995–2003. doi:10.1021/nn103047r

48. Liu X, Tao H, Yang K, et al. Optimization of surface chemistry on single-walled carbon nanotubes for in vivo photothermal ablation of tumors. *Biomaterials*. 2011;32(1):144–151. doi:10.1016/j.biomaterials.2010.08.096